Low-lying Gamow-Teller states in ^{92}Nb

S. M. Grimes
Ohio University, Athens, Ohio 45701

R. W. Bauer, J. D. Anderson, V. R. Brown, B. A. Pohl, and C. H. Poppe*
Lawrence Livermore National Laboratory, University of California, Livermore, California 94550

V. A. Madsen
Oregon State University, Corvallis, Oregon 97331

R. Langkau, W. Scobel, and S. Stamer
I. Institut für Experimentalphysik, University of Hamburg, Federal Republic of Germany
(Received 31 October 1995)

Cross sections for the (p,n) reaction on targets of ^{90}Zr and ^{92}Zr have been measured at 26 MeV. Our resolution for these measurements was better than 200 keV and allowed the observation of numerous 1^+ states in ^{92}Nb below 7 MeV excitation. Our analysis is focused on states below the primary Gamow-Teller state and shows a fragmentation of the Gamow-Teller strength that is only partially accounted for by three different model calculations: a quasiparticle model, a shell model, and a random-phase approximation calculation. All three models yield predictions which include appreciable strength between 3 and 7 MeV excitation, but fail to describe our experimental results in detail. [S0556-2813(96)03206-2]

PACS number(s): 24.30.Cz, 25.40.Kv, 27.60.+j

I. INTRODUCTION

The connection between Gamow-Teller and Fermi β decay matrix elements for light nuclei and the (p,n) charge exchange reaction has been used for studying the isovector part of the effective nucleon-nucleon interaction for about two decades (see, e.g., Refs. [1–4]). At intermediate energies (100–200 MeV) Goodman and collaborators [3,5] and others (e.g., Sterrenberg *et al.* [6] and Anderson *et al.* [7]) have shown that the spin exchange part of the effective force is dominant. This has enabled Goodman and co-workers [5,8,9] to extract the Gamow-Teller β decay strength from the zero-degree (p,n) reaction. The uncertainties in extracting absolute matrix elements from these data are discussed by Taddeucci *et al.* [10].

The (p,n) reaction technique has an obvious advantage over β decay studies in that states not available as initial states in β decay can be examined as final states in (p,n) reactions. Two obvious disadvantages in the (p,n) reaction are the possible presence of non-Gamow-Teller contributions in the (p,n) reaction (even at forward angles) and the difficulty of obtaining good resolution to resolve low-lying states. In order to minimize difficulties with non-Gamow-Teller contributions, it is advantageous to make measurements at energies above 100 MeV. This complicates the problem of obtaining good resolution, since as pointed out by Goodman [9] a 130 m flight path is needed for 300 keV resolution at 160 MeV. Even this resolution, which allows study of the giant Gamow-Teller state, does not provide good separation for the low-lying states.

One alternative is to utilize the $(^3\mathrm{He},t)$ reaction. Although it is thought that multistep processes complicate the interpretation of this reaction at low energies, it has been shown that at energies above 150 MeV/nucleon the $(^3\mathrm{He},t)$ results agree well with those from the (p,n) studies at the same energy per nucleon [11]. A recent investigation of the $(^3\mathrm{He},t)$ reaction on the stable isotopes of tin [12] has achieved a resolution of 80 keV. Even with this resolution the authors point out an uncertainty of about 250 keV in the centroid of the primary Gamow-Teller peak caused by uncertainties in subtracting nonresonant background; this in spite of the fact that the centroid of each state was determined to an accuracy of 30 keV.

Theoretical studies [13] of the Gamow-Teller resonance have predicted a fragmentation of the Gamow-Teller strength. The primary peak (type I) is expected to come from transitions to states of the type $(l-1/2)_p(l+1/2)_n^{-1}$ which would be expected to be slightly above the isobaric analog resonance (IAR). In a nucleus in which the $l+1/2$ or $l-1/2$ orbit for protons is at least partly empty and the corresponding orbit for neutrons is at least partly full, transitions of the type (type II) $(l\pm1/2)_p(l\pm1/2)_n^{-1}$ are possible; these can couple to $I^\pi=1^+$ and will be lower in energy than the first type listed. Finally, states of the type (type III) $(l+1/2)_p(l-1/2)_n^{-1}$ can occur at an even lower energy, and in some cases could include the ground state. The number of such states and the total strength are very sensitive to the amount of configuration mixing, since for an ideal closed-shell nucleus only the collective Gamow-Teller state (type I) will be seen. In a real nucleus, states will generally be mixtures of the three types.

The present measurements were undertaken to see if lower-energy (p,n) measurements could provide more information about the low-lying Gamow-Teller strength. Previous

*Present address: Office of the President, University of California, Oakland, CA 94612.

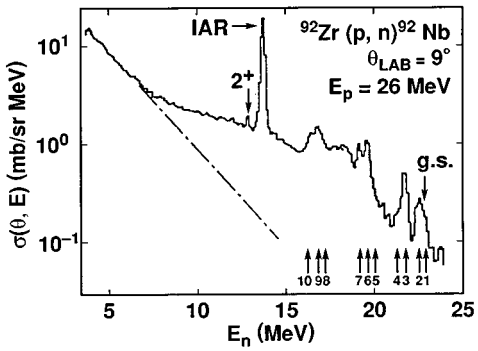

FIG. 1. Neutron energy spectrum for ^{92}Zr$(p,n)^{92}$Nb at $E_p=26$ MeV. The levels for which angular distributions could be obtained are labeled 1 through 10. The positions of the ground, IAR, and 2^+ IAR states in ^{92}Nb are also indicated. The dash-dotted line shows the extrapolation of the exponential decrease in the low-energy neutron spectrum from compound nuclear decay.

attempts to extract absolute Gamow-Teller matrix elements from zero-degree cross sections have been unsuccessful [14] as shown in a theoretical analysis [15]. We therefore restrict our efforts to see if we can deduce the fractionation of the strength to the single state in ^{90}Nb into low-lying states in ^{92}Nb. While the low-energy zero-degree (p,n) cross sections are not directly proportional to the Gamow-Teller strength, there exists a strong dependence.

The target in our experiment was ^{92}Zr and the (p,n) reaction was studied at 26 MeV. An earlier investigation of the (p,n) reaction on the zirconium isotopes [16] at this energy showed that the angular distribution of the (p,n) reaction on ^{90}Zr to the 1^+ state at 2.13 MeV was identical in shape to the forward angular distribution for the analog transition. Other Zr isotopes showed evidence for 1^+ states as well. We have repeated the measurement of the (p,n) cross section on ^{90}Zr and ^{92}Zr with better energy resolution at the cyclotron facility of the University of Hamburg. Section II of this paper presents the experimental procedure and experimental results. In Sec. III we compare our results with those derived from several model calculations, and Sec. IV gives a summary and our conclusion.

II. EXPERIMENTAL PROCEDURE AND RESULTS

The experiment was carried out at the Hamburg Isochronous Cyclotron Facility. The energy of the incident proton beam was 26.0 ± 0.1 MeV in this series of measurements. The beam impinged on self-supporting metallic target foils of highly enriched ($>95\%$) zirconium ^{90}Zr with a thickness of 6.2 mg/cm^2 and ^{92}Zr with a thickness of 5.3 mg/cm^2. A beam burst separation of 829 ns was obtained by effectively ($>99.8\%$) suppressing 15 out of 16 bursts with an external deflection system. The resulting beam intensity of approximately 80 nA allowed one set of measurements to be completed within 4 h with a charge of typically 1 mC accumulated in the heavily shielded Faraday cup. A schematic layout of the beamline together with the target chamber and the neutron time-of-flight setup is shown in Fig. 1 of Ref. [17].

The standard Hamburg neutron time-of-flight (TOF) setup, consisting of eight detectors and three possible target

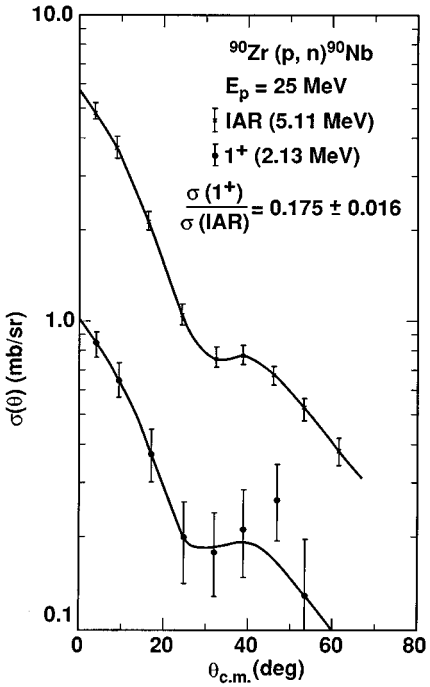

FIG. 2. Angular distribution for the ^{90}Zr$(p,n)^{90}$Nb reaction to the IAR (5.11 MeV) and 1^+ (2.13 MeV) levels at 25 MeV proton bombarding energy. The absolute cross sections are shown. The solid curves are provided as a guide to the eye.

positions, covered an angular range of $3°\leqslant\theta_{lab}\leqslant177°$ with 24 roughly equidistant positions. Details of this experimental setup and its performance in neutron spectroscopy have been described previously [18,19]. For the present experiment this setup was modified to improve the neutron resolution for the angles $\theta_{lab}\leqslant60°$. These modifications as well as the characteristics of the time-of-flight detectors used in this experiment have been presented in Ref. [17]. With these improvements effective n-γ pulse-shape discrimination was obtained and an overall neutron energy resolution ranging from 125 to 200 keV, depending on the individual detectors, was achieved for the isobaric analog transitions ($E_n\approx12.5$ MeV).

A representative neutron spectrum for a detector at the flight path of approximately 20 m is shown in Fig. 2 of Ref. [17]. The conversion into absolute energy spectra, achieved by using time calibrations derived from the positions of the (strongly reduced) γ peaks from two subsequent beam bursts, and the detector efficiency calculations have been described previously [17]. The uncertainties resulting from target inhomogeneities and impurities ($<5\%$), incomplete beam current integration ($<3\%$), and detector efficiency ($\leqslant4\%$) lead to a minimum uncertainty $\Delta\sigma/\sigma=7\%$ of the differential cross sections. Additional contributions to the uncertainty are due to counting statistics and peak integration (see below).

A neutron energy spectrum for the ^{92}Zr (p,n) ^{92}Nb reaction is shown in Fig. 1. The characteristic features of the spectrum are a number of neutron peaks superimposed on the neutron continuum. The extrapolation of the exponential decrease in the low-energy neutron spectrum from compound nuclear decay is shown as a dash-dotted line. Details of the ^{92}Zr (p,n) spectrum will be discussed below. Measurements

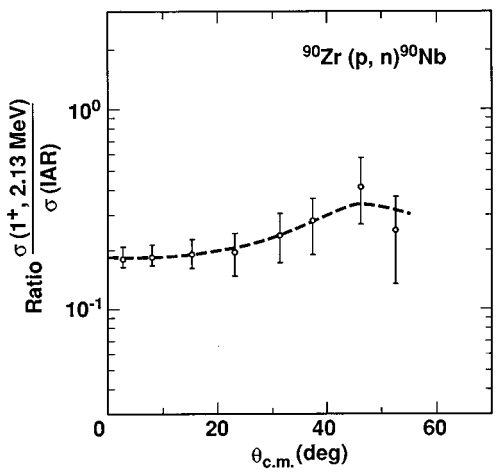

FIG. 3. Ratio of the cross sections for the ^{90}Zr$(p,n)^{90}$Nb reactions to the 1^+ (2.13 MeV excitation) state divided by the IAR cross section (5.11 MeV level) at 25 MeV proton bombarding energy. (The same 3° ratio is obtained at 26 MeV.) The dashed curve is provided as a guide to the eye.

at 3°, 9°, and 15° were made with a 20 m flight path and spectra were also obtained at angles of 27°, 33°, 46°, and 53° at a flight path of 7.5 m. Because of the energy dependence of the effective nucleon-nucleon potential [4,20], the lower energy of 26 MeV in the current experiment reduces the cross section ratio of Gamow-Teller transitions to Fermi transitions below that seen at $E_p > 100$ MeV (e.g., the investigations by Goodman and collaborators [3,5]). The better energy resolution available at this lower bombarding energy may compensate for this limitation.

For the ^{90}Zr (p,n) ^{90}Nb reaction, one strong 1^+ transition was observed which populates the state at the excitation energy of 2.13 MeV. An additional 1^+ transition with a strength of about 30% of the 2.13 MeV state has been observed at 0.38 MeV excitation in the (^{3}He,t) reaction [21]. However, the 2.13 MeV transition and the analog transition at 5.11 MeV were the only two strong transitions observed in the neutron time-of-flight spectrum of the (p,n) reaction. These latter two groups had very similar angular distributions, supporting our assumption that the 1^+ states are predominantly populated by $\Delta L = 0$ transitions rather than $\Delta L = 2$. Contributions from $\Delta L = 1$ would be forbidden by parity restrictions if the final state were a 1^+ state. Figure 2 shows the angular distributions obtained for the analog and the 1^+ state (at 2.13 MeV excitation) in ^{90}Nb.

Figure 3 presents a ratio of the cross sections for the transition to the 1^+ state to that to the analog state in ^{90}Nb. A ratio of 0.175 ± 0.016 is observed for $\theta_{\text{c.m.}} = 3°$. This number is used in our analysis below when scaling from ^{90}Nb to ^{92}Nb. On close inspection of Fig. 3 one can also discern a slight rise of the ratio at the larger angles, which suggests the possibility of some $L = 2$ admixture to the predominant $L = 0$ contribution in the transition to the 1^+ level.

The energy spectrum of neutrons emitted at 9° for 26 MeV protons on ^{92}Zr was shown in Fig. 1. The levels used in our analysis are numbered 1–10. The neutron peaks which were subsequently identified as due to the excitation of 1^+ levels (together with their corresponding residual excitation energies) are the peaks numbered 3 (at 1.09 MeV excitation), 6 (at 3.15 MeV), 7 (at 3.53 MeV), 9 (at 5.92 MeV), and 10 (at 6.28 MeV), with peak number 4 (at 1.48 MeV) probably also populating a 1^+ level. Note that neutrons from the 2.13 MeV level in ^{90}Nb fall between levels 9 and 10. The levels labeled 1 and 2 represent the cluster of states from 0 to 500 keV excitation. From the change of shape of this cluster as a function of angle it was clear that at least two different states are strongly excited. In order to fit the changes in shape of the clusters 6,7 and 9,10 as a function of angles, levels 5 and 8 were also needed.

Comparison of these peaks with the level scheme presented in Nuclear Data Sheets [22] supports our interpretation of these results. Both the peak at 1.09 and the one at 1.48 MeV are at energies corresponding to known 1^+ states. Unfortunately, these are the only two levels in the tabulation which have been assigned 1^+ as the spin and parity, so a more detailed comparison cannot be made.

To extract peak cross sections we worked from the time-of-flight spectra using the peak-fitting code FITEK [23]. This program is highly interactive and is used to search for peaks and determine their shapes, centroids, and areas as well as to fit the background underneath them. The peak shape was generally derived from a well resolved pronounced neutron peak, such as the IAR peak (see Fig. 1), which was found to be a skewed Gaussian with a small tail toward later times (toward lower neutron energies). This peak shape was held fixed (only the width was adjusted for different neutron energies) when searching for less pronounced peaks and when integrating under the peaks. Kinematics were also used to fix the position of minor peaks with respect to neighboring larger peaks. The uncertainty of the integral under a peak minus the background, also determined by FITEK, included the statistical errors of the signal and the background as well as the error due to the deviation of the individual points from the skewed Gaussian imposed by the program. Thus the total calculated error includes both the statistics and a measure of the goodness of the fit of the data to the imposed Gaussian shape. This total error for the cross section was then combined with the systematic uncertainty of 7% discussed earlier. The background generated by FITEK is completely empirical, depending only on the fitting of the Gaussian shaped peaks.

Figure 4 shows an example of one of the FITEK spectra covering an excitation energy from 3 to 7 MeV (approximately) in ^{92}Nb. During this first pass the major features of the spectrum are being fitted. During subsequent passes we could select the number of peaks, fix their locations, vary the background, compare several spectra from different angular positions, etc., to obtain optimum values for the energies of the peaks and the integrals under the peaks at minimum errors determined by FITEK. We obtain the best values for the 3° and 9° spectra, where the 1^+ signals were largest. For the larger angles, where the 1^+ cross sections were smaller, we needed to fix the relative spacing of the levels to obtain consistent fits.

Note that the difficulties we encounter when analyzing our data using FITEK are very similar to those encountered in fitting (^{3}He,t) or (p,n) spectra at higher energies. In each of these situations, a large ''background'' of particles due to ''non-Gamow-Teller'' processes, e.g., excitation of the

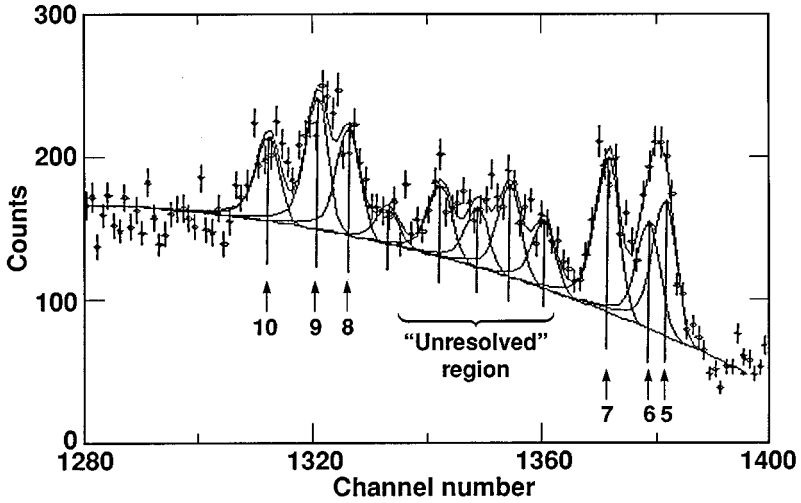

FIG. 4. Representative neutron TOF spectrum of transitions to low-lying states in the ^{92}Zr (p,n) ^{92}Nb reaction at 26 MeV proton energy for the laboratory angle of 9°. The solid curve through the data points and the background curve under the peaks are examples of the fits generated by the FITEK program. The numbers below the peak refer to the labels of levels in Fig. 1. The ''unresolved'' region is near ~4.75 MeV excitation (see Table I below). The abscissa is linear in channel numbers and increasing time is toward the left.

higher multipoles and preequilibrium neutron decay, must be subtracted from the peaks. The ultimate errors in both areas and centroids of these peaks are more dependent on background subtraction than on more conventional sources of error like energy calibration, efficiency determination, or counting statistics. The fact that our resolution is better than that for the high-energy (p,n) studies roughly compensates for the lower Gamow-Teller cross sections at this energy. The challenge of background subtraction places a premium on studying the Gamow-Teller strength in a number of different experiments.

In Fig. 5 we present cross sections for ten levels excited in the ^{92}Zr$(p,n)^{92}$Nb reaction, including the IAR transition (at 9.03 MeV excitation) and five levels identified as 1^+ levels ranging in energy from 1.09 to 6.28 MeV excitation (shown in the left side of Fig. 5). The angular distributions for levels 1, 2, 5, and 8 (shown on the right-hand side of Fig. 5) do not display the $L=0$ characteristics and thus do not specify 1^+ levels. In Fig. 6 we plot the ratio of the 1^+ to the ^{92}Zr (p,n) IAR cross section for five 1^+ levels. For the 1^+ levels closest in energy to the IAR, 9 (5.92 MeV) and 10 (6.28 MeV), the ratio to the IAR is a constant as a function of angle (3°–15°) to ±10%. For the lower-lying levels, e.g., 3 (1.09 MeV), the 1^+ angular distribution is more forward peaked, as one would expect with the smaller momentum mismatch.

Even at intermediate energies the direct interpretation of zero-degree cross sections as a measure of the Gamow-Teller

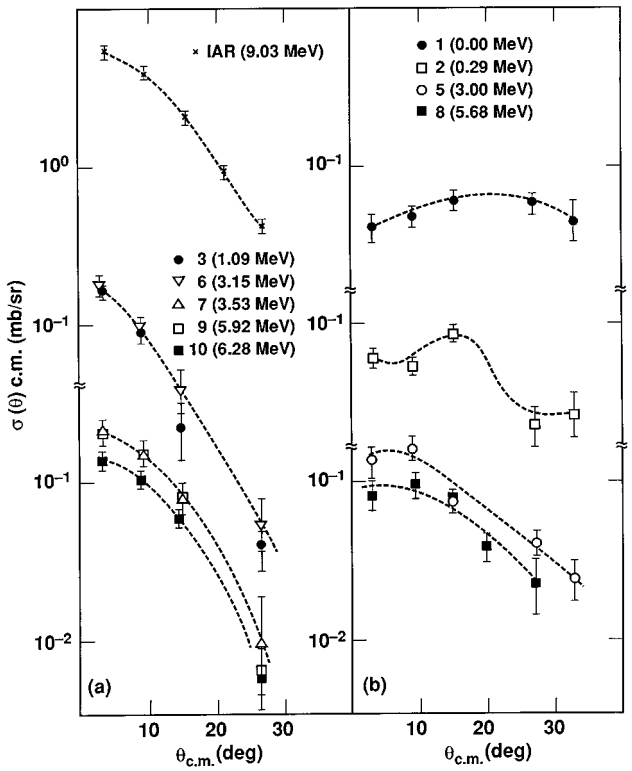

FIG. 5. Angular distribution for the ^{92}Zr$(p,n)^{92}$Nb reaction to the ''resolved'' low-lying levels at 26 MeV proton bombarding energy. The absolute cross sections are shown. The dashed curves are provided as a guide to the eye.

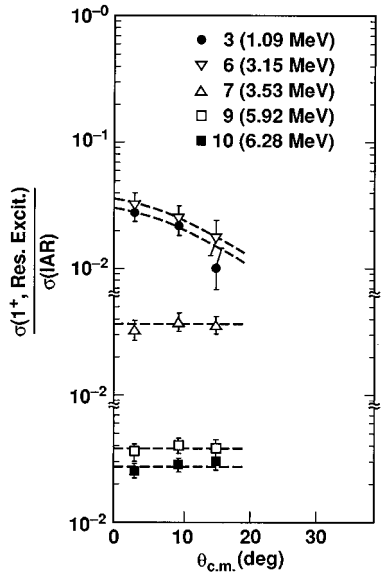

FIG. 6. Ratio of the cross sections for the ^{92}Zr$(p,n)^{92}$Nb reaction to the identified 1^+ levels divided by the IAR cross section (9.03 MeV level) at 26 MeV proton bombarding energy. The dashed curves are provided as a guide to the eye.

TABLE I. Low-lying Gamow-Teller transition strength in ^{92}Nb. The estimates of the Gamow-Teller strength B(GT) from the ^{92}Zr$(p,n)^{92}$Nb reaction are normalized to the ^{90}Zr$(p,n)^{90}$Nb reaction [8]. (The ''Ratio to IAR'' refers to the ratio of the cross sections for the respective Gamow-Teller transition divided by the isobaric analog resonance cross section.)

Nucleus	Residual excitation (MeV)	$\sigma(3°)$ (mb/sr)	Ratio to IAR ($\times 100$)	B(GT)
^{90}Zr$(p,n)^{90}$Nb	2.13	0.85 ± 0.08	17.5 ± 1.6	1.8 [a]
	5.11 (IAR)	4.85 ± 0.25		
^{92}Zr$(p,n)^{92}$Nb	1.09	0.159 ± 0.011	3.0 ± 0.2	0.3
	3.15	0.178 ± 0.034	3.3 ± 0.6	0.4
	3.53	0.187 ± 0.019	3.5 ± 0.35	0.4
	($\sim$4.75)		(3.4 ± 1.7) [b]	(0.4) [b]
	5.92	0.200 ± 0.022	3.7 ± 0.4	0..5
	6.28	0.147 ± 0.021	2.7 ± 0.4	0.3
	9.03 (IAR)	5.38 ± 0.11		
			Sum [c] $=19\pm4$	
			(22 ± 4) [d]	
			Scaled from ^{90}Zr$=21\pm2$	

[a]Taken from Bainum *et al.* [8].

[b]Unresolved, estimated strength at $\sim$4.75 MeV excitation (see Ref. [24]).

[c]In the sum we have corrected for the differences in the neutron momentum relative to ^{90}Zr.

[d]Includes estimated strength at $\sim$4.75 MeV excitation.

strength is uncertain to a factor of 2 [10]. This uncertainty is so large even for isotopes of the same element, e.g., ^{13}C vs ^{14}C. These fluctuations are reduced to the 20–30 % level by normalizing to the Fermi matrix element in the same nucleus. At intermediate energies all the data are well described by [10]

$$\left(\frac{\sigma(0°,\mathrm{GT})}{B(\mathrm{GT})}\right)\left(\frac{\sigma(0°,F)}{B(F)}\right)^{-1}=\left(\frac{E_p}{E_0}\right)^2, \qquad (1)$$

neglecting kinematic factors close to 1. Here, E_0 is a constant equal to 55 MeV for the high-energy (p,n) data, E_p is the incident proton energy, $\sigma(0°,\mathrm{GT})$ is the zero-degree cross section to the individual 1^+ level, B(GT) is the corresponding Gamow-Teller transition strength, $\sigma(0°,F)$ is the IAR cross section, and $B(F)$ is equal to $(N-Z)$. For ^{90}Zr at 26 MeV, using $B(\mathrm{GT})=1.8$ for the 2.13 MeV level [8], we obtain a ratio of 0.9. This is a factor of 4 larger than the empirical value obtained for Eq. (1) at intermediate energies, which also describes light nuclei in our energy region. This is not too surprising in that the momentum transfer characteristic of the Zr(p,n) process is quite large compared to the light nuclei. A similar energy dependence for E_0 arises in a macroscopic description due to the energy dependence of the isovector optical potential V_1, e.g., $V_1=100-0.6E_p$. Uncertainties due to momentum mismatch and other distortion effects are expected to be minimized by taking these ratios and by normalizing to the measured ^{90}Zr Gamow-Teller transition strength.

We also correct for phase space in that the cross sections are divided by the relative momentum, with respect to the IAR, of the outgoing neutron. Our estimates of the Gamow-Teller transition strengths obtained from the normalized ^{92}Zr (p,n) reaction are listed in Table I [24]. The cross section errors listed include only errors from the data analysis. In column 4 (labeled ''Ratio to IAR'') we have summed the normalized cross section strength found for ^{92}Zr and compare it to the ^{90}Zr strength scaled by $N-Z$. It is surprising and perhaps merely fortuitous that the summed strength agrees within 10% with our expectation, i.e., ^{92}Zr $\approx[(N-Z)_{92}/(N-Z)_{90}]^{90}$Zr. From the discussion that follows it should be clear that 30–50 % uncertainties should be attached to the ratio of these strengths as well as to their absolute values. Since our procedure sums to give reasonable results, we also list our estimate of the Gamow-Teller strength B(GT) in column 5 of Table I [labeled ''B(GT)''].

Before interpreting these results we discuss possible additional uncertainties. At these lower bombarding energies, the Fermi type transitions ($\Delta L=0$, $\Delta S=0$) dominate and neutrons from statistical and preequilibrium processes to some extent [25,26] obscure the collective Gamow-Teller resonance which should occur at about 10 MeV neutron energy in Fig. 1. Because the 1^+ transitions we are attempting to study are located in regions of level density where we could not resolve the individual levels, we also measured the ^{89}Y $(p,n)^{89}$Zr(0.58 MeV) reaction. This is a $1/2^-$ to $1/2^-$ transition which is well resolved from the $9/2^+$ ground state and from the second excited state at 1.1 MeV. Its angular distribution had the same shape as the analog and yielded a ratio of $(1.0\pm0.3)\times10^{-2}$. We assume that the background cannot exceed twice this error. As a percentage of the analog state cross section, we therefore conclude that backgrounds from nondirect processes are less than 0.6×10^{-2}.

The major uncertainty is the contribution from the $L=2$ moment of the two-body force. At these low bombarding energies space exchange (knockout reactions) significantly

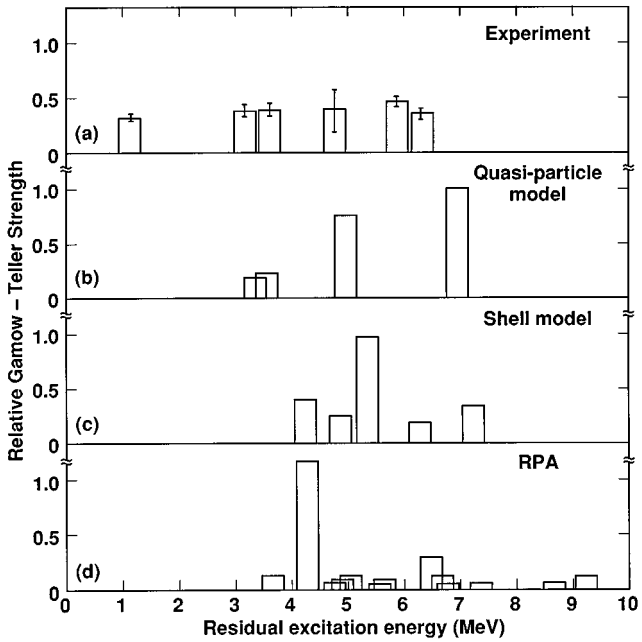

FIG. 7. Comparison of the measured and calculated low-lying Gamow-Teller strength distributions for ^{92}Nb. For a discussion of the three different model calculations, refer to Sec. III.

enhance the $L=2$ moments. For the spin exchange part of the two-body force we also have a large tensor contribution. Both contribute to a $\Delta I=1$, $\Delta S=1$, $\Delta L=2$ component to the (p,n) reaction which is not proportional to the Gamow-Teller β decay matrix element. At intermediate energies these $\Delta L=2$ contributions are clearly identified by their characteristic angular distributions. However, at low bombarding energies the optical distortions tend to obscure the differences in angular distributions. We use the angular distributions of the analog 2^+ state, which proceeds via a two-step process, as measure of the uncertainty of the $L=2$ contribution and conclude that this contributes to an overall uncertainty of less than 30%. Tensor contributions to the $L=0$ amplitudes from $L=2$ nuclear transitions, however, cannot be distinguished from $L=0$ Gamow-Teller amplitudes by their angular distributions.

III. COMPARISON OF RESULTS WITH CALCULATIONS

We now compare our Gamow-Teller strength distribution in ^{92}Nb (listed in Table I) with several model calculations. These calculations include a quasiparticle calculation, a shell model calculation, and a random-phase approximation (RPA) calculation. Details of these calculations are presented in this section and the results are summarized in Fig. 7.

A. Quasiparticle calculations

A calculation of the fragmentation of Gamow-Teller strength in spherical nuclei has been published by Gaponov and Lyutostanskii [13]. This model is quite simple and does not include fine details about the two-body force that are included in the RPA and shell model calculations, but such a schematic model is easy to apply and can help us understand the systematics of Gamow-Teller fragmentation, even if it does not yield a highly accurate representation. The primary Gamow-Teller strength is expected to appear in a giant Gamow-Teller state. This state is expected to consist of coherent contributions from configurations of the type $(l-1/2)_p(l+1/2)_{\bar{n}}$. For zirconium isotopes, it would be expected that a dominant term would be the $(g_{7/2})_p(g_{9/2})_{\bar{n}}$ configuration, although the $(d_{3/2})_p(d_{5/2})_{\bar{n}}$ component will play a role if significant neutron occupancy of the $d_{5/2}$ state is present. This giant state should be found above the isobaric analog state by about the spin-orbit splitting. Because of our low bombarding energy, this state falls in the region of high background. Its large width combined with the background causes it to be hidden in our measurements. Higher still in the spectrum is the analog of the giant $M1$ state in the parent. This state was also not seen in our measurements.

The remaining Gamow-Teller states should be primarily of the types II and III, i.e., consisting of configurations $(l\pm 1/2)_p(l\pm 1/2)_{\bar{n}}$ or $(l+1/2)_p(l-1/2)_{\bar{n}}$. Without considering mixing caused by the two-body force, type II states ought to be lower in energy than the giant Gamow-Teller state by about the spin-orbit splitting and type III states lower than the type II states by the same amount. Neither type is likely to be pure in a real nucleus and both might have portions of type I states as well. All these types could be suppressed for certain nuclei.

As an example, consider a nucleus whose highest two orbits are $g_{9/2}$ and $g_{7/2}$ and assume both are completely filled with both neutrons and protons. No strength from any of these Gamow-Teller processes will be present. As protons are removed from the $g_{7/2}$ orbit, strength will be seen from Gamow-Teller processes of types I and II, but not type III, since this requires vacancies in the $g_{9/2}$ shell for protons. Only if some vacancies in both $g_{9/2}$ and $g_{7/2}$ orbits for protons occur, and some neutrons are present in the $g_{9/2}$ and $g_{7/2}$ orbits, will all three types be present. Similarly, if the $g_{7/2}$ orbit is emptied of neutrons, contributions of type III will be suppressed. If the ground state of ^{90}Zr were actually $(g_{9/2})_n^{10}$, only type I and type II contributions would be present.

Gaponov and Lyutostanskii use a quasiparticle model and evaluate the appropriate Gamow-Teller matrix element for transitions between these states. For ^{92}Nb, their predictions are shown in Fig. 7. Gamow-Teller strength is predicted to appear in the giant state as well as in four states below the giant state. These four energies range from 3.37 to 6.97 MeV. The principal flaw in their prediction is the absence of any strength at 1 MeV. The experimental information on the strength in this region seems solid, since there is less ''background'' in this region than at higher energies, and there is a known 1^+ state at this energy. This calculation also gives more strength between 5 and 7 than between 3 and 5 MeV, while the data show roughly comparable strength in these two regions.

B. Shell model calculations

Another theoretical calculation was taken from the shell model. Mathews, Bloom, and Hausman [27] have described a calculation of the Gamow-Teller strength in ^{90}Nb using the shell model. This calculation utilized the $2p1g2d$ basis and the Petrovich-McManus-Madsen-Atkinson (PMMA) Hamil-

tonian [28]. Relatively good agreement with the Gamow-Teller strength observed in measurements at 160 MeV was obtained [8]. However, the resolution was poorer than in the present experiment, and ^{90}Zr probably has a simpler configuration in its ground state, which would lead to less fragmentation of the Gamow-Teller strength. The spectrum obtained experimentally had only the giant Gamow-Teller state and one other Gamow-Teller state, while the experimental results obtained here for ^{92}Zr are more fragmented.

The conventional technique used to calculate a strength distribution with the shell model is to diagonalize the Hamiltonian in both the target and residual nucleus systems. The $M1$ strength in each state is directly obtained by evaluating the matrix element between that final state and the initial state.

A much more powerful technique has been developed [29]. This procedure involves diagonalizing the Hamiltonian to obtain the ground state of the target. The Gamow-Teller operator is then applied to this state $|\Phi_0\rangle$ to form the vector $|V_{\rm GT}\rangle$,

$$|V_{\rm GT}\rangle = {\rm GT}|\Phi_0\rangle. \tag{2}$$

This vector is then used as the start vector in a Lanczos calculation [29]. Each step in the Lanczos process produces one more orthogonal vector. After N stages, diagonalization of the Hamiltonian results in N pseudoeigenfunctions whose eigenvectors appear in the start vector with weights such that the lowest $2N-1$ energy moments of the start vector are reproduced. Clearly, the process eventually yields all eigenvalues, but if stopped after a few stages, peaks can be generated which provide an envelope of the strength distribution. If the experiment yields more peaks than the theoretical calculation, additional iterations can be run to further divide the strength. The ultimate limit will be the number of eigenstates in the basis, which for Zr is far more than the number of peaks seen experimentally.

A calculation using this technique was made for the ^{92}Zr$(p,n)^{92}$Nb reaction [30]. This calculation used the same single-particle energies and two-body matrix elements as the ^{90}Zr calculations of Ref. [27].

The results of this calculation are shown in Fig. 7. The shell model calculation puts Gamow-Teller strength in five states below the analog and giant Gamow-Teller state. The strength distribution is at slightly too high an energy and fails to predict any strength near 1 MeV. The shell model calculation, however, does predict that the strength in this region is fragmented, and not concentrated in one peak as in ^{90}Nb.

C. RPA calculations

The 1^+ two-quasiparticle spectrum in ^{92}Nb was calculated with the Oregon State–Livermore random-phase approximation code [31], which uses a separable multipole particle-hole interaction.

The strength of the interaction is determined by choosing the $V_{\sigma\tau}$ strength to be $\frac{2}{3}V_\tau$, the ratio given by the PMMA interaction [28]. This procedure places the analog strength at about 10.2 MeV and the giant Gamow-Teller state at 11.3 MeV. With the same strength, the analog in ^{90}Zr is at 9.2 MeV and the GT giant resonance is at 11.2 MeV.

All single-particle states in harmonic oscillator shells $N=0$ to 7 plus the $k_{17/2}$ state were included. The harmonic oscillator parameters in the Nilsson level scheme were chosen so the geometrical mean for neutron and proton is $\hbar\omega = 41/A^{1/3}$ with the ratio of neutron to proton nuclear radii chosen to be 1.03. Appropriate shifts of the $p_{3/2}$ proton level and the $N=4$ neutron levels and the pairing calculations have been described in an earlier paper [32].

Figure 7 shows the RPA-based GT strengths in comparison to the experimental (p,n) data and the strengths calculated from the quasiparticle model and the shell model. According to the RPA calculation more than half of the GT strength below 9 MeV in ^{92}Nb was found to lie in one particle-hole excitation at 4.2 MeV. This state is primarily a $(g_{9/2})_p(g_{9/2})_n^-$ type II configuration, which also occurs in ^{90}Zr(p,n). This is the spin-orbit partner transition to the GT giant resonance, which is predominantly a $(g_{7/2})_p(g_{9/2})_n^-$ type I transition, accounting for its higher energy. The lower-energy type III particle-hole configuration is nearly nonexistent in ^{92}Zr as well as in ^{90}Zr because of the very small occupancy of the $g_{7/2}$ neutron level.

The RPA calculation has its strength primarily in one strong excitation at 4.2 MeV, in contrast to the experimental cross section distribution, which shows six peaks of more or less equal strength.

The difference between the RPA and the shell model calculations can be the result of two separate factors. The shell model includes many-particle many-hole contributions, and thus is limited to a small number of orbits because of basis-size limitations. On the other hand, the RPA calculation includes only one-particle one-hole contributions allowing a bigger single-particle basis. Depending on whether the multiple-particle multiple-hole contributions are more important than the inclusion of more single-particle orbits, either model could produce better results. A further difference between the two calculations is that the shell model uses a Yukawa form factor, while the RPA was made using a separable multipole interaction with surface-peaked radial form factors. In the present comparison the shell model takes into account more low-lying configurations and thus distributes the low-lying strength more evenly, in better quantitative agreement with experiment.

IV. SUMMARY AND CONCLUSION

The neutron spectrum produced by 26 MeV proton bombardment of ^{92}Zr has been measured at forward angles with emphasis on good resolution for low-lying states. A number of peaks have been found to have angular distributions similar to that for the isobaric analog state. Six such peaks were identified as due to 1^+ states or envelopes of 1^+ strength. Some indication that our low-energy results may be consistent with measurements above 100 MeV is provided by two recent papers [33,34] on the ^{11}B(p,n) reaction. A paper by Taddeucci *et al.* [33] has examined the reaction and its analyzing power at energies above 150 MeV, while Grimes *et al.* [34] studied it at 26 MeV. The results of these two measurements are in good general agreement on the strength distribution, providing some justification for our interpretation of the Zr results obtained at 26 MeV.

Relative strengths of our measured Gamow-Teller peaks

were determined to about $\pm 30\%$. Comparison of these strengths was made with a quasiparticle model, and with a RPA and a shell model calculation. The more detailed RPA and shell model predictions show somewhat more fragmentation than the simpler quasiparticle model, as expected. Each of these methods yielded a prediction which did include strength between 3 and 7 MeV, but failed to describe our results in detail. The tendency was to miss the strength at 1 MeV and to clump the strength in one or two states between 3 and 7 MeV, while the data show a broader spread of strength in this energy region. Further good resolution (p,n) measurements at intermediate energies would be helpful in clarifying the low-energy Gamow-Teller spectrum. In addition, it would be desirable to check the results obtained here at higher energies to help determine how effective measurements at energies between 20 and 30 MeV can be at determining Gamow-Teller strength.

A study by Gaarde, Larsen, and Rapaport [35] has found that approximately 20% of the total Gamow-Teller strength is below the giant Gamow-Teller state. As the present results point out, the details of the spreading of Gamow-Teller strength are not completely described by current nuclear models. An accurate description of the Gamow-Teller distribution will obviously require a reliable procedure for describing configuration mixing. Our results indicate that the small peaks at low excitation energy are particularly difficult to reproduce and represent a greater challenge to theory than the description of the giant resonance itself.

ACKNOWLEDGMENTS

This work was performed under the auspices of the U.S. Department of Energy by the Lawrence Livermore National Laboratory under Contract No. W-7405-ENG-48. It was also supported at the University of Hamburg by the Germany Federal Ministry of Research and Technology (BMFT) under Contract No. 06-HH-142.

[1] J. D. Anderson, C. Wong, and V. A. Madsen, Phys. Rev. Lett. **24**, 1074 (1970).

[2] S. M. Austin, in *The Two Body Force in Nuclei*, edited by S. M. Austin and G. M. Crawley (Plenum, New York, 1972), p. 285.

[3] C. D. Goodman, C. A. Goulding, M. B. Greenfield, J. Rapaport, D. E. Bainum, C. C. Foster, W. G. Love, and F. Petrovich, Phys. Rev. Lett. **44**, 1955 (1980).

[4] W. G. Love, K. Nakayama, and M. A. Franey, Phys. Rev. Lett. **59**, 1401 (1987).

[5] See C. Goodman, in *The* (p,n) *Reaction and the Nucleon-Nucleon Force*, edited by C. D. Goodman, S. M. Austin, S. D. Bloom, J. Rapaport, and G. R. Satchler (Plenum, New York, 1980), p. 170; W. G. Love, *ibid.*, pp. 30 and 42; F. Petrovich, *ibid.*, p. 135.

[6] W. A. Sterrenberg, S. M. Austin, U. E. P. Berg, and R. DeVito, Phys. Lett. **91B**, 337 (1980).

[7] B. D. Anderson, T. Chittrakarn, A. R. Baldwin, C. Lebo, R. Madey, R. J. McCarthy, J. W. Watson, B. A. Brown, and C. C. Foster, Phys. Rev. C **31**, 1161 (1985).

[8] D. E. Bainum, J. Rapaport, C. D. Goodman, D. J. Horen, C. C. Foster, M. B. Greenfield, and C. A. Goulding, Phys. Rev. Lett. **44**, 1751 (1980).

[9] C. D. Goodman, Can. J. Phys. **65**, 549 (1987).

[10] T. N. Taddeucci, C. A. Goulding, T. A. Carey, R. C. Byrd, C. D. Goodman, C. Gaarde, J. Larsen, D. J. Horen, J. Rapaport, and E. Sugarbaker, Nucl. Phys. **A469**, 125 (1987).

[11] H. Akimune, I. Daito, Y. Fijita, M. Fujiwara, M. B. Greenfield, M. N. Harakeh, T. Inomata, J. Jänecke, K. Katori, S. Nakayama, H. Sakai, Y. Sakemi, M. Tanaka, and M. Yosoi, Nucl. Phys. **A569**, 245c (1994).

[12] K. Pham, J. Jänecke, D. A. Roberts, M. N. Harakeh, G. P. A. Berg, S. Chang, J. Liu, E. J. Stevenson, B. F. Davis, H. Akimune, and M. Fujiwara, Phys. Rev. C **51**, 526 (1995).

[13] Yu. V. Gaponov and Yu. S. Lyutostanskii, Fiz. Elem. Chastits At. Yadra **12**, 1324 (1981) [Sov. J. Part. Nucl. **12**, 528 (1981)].

[14] H. Orihara, C. D. Zafiratos, S. Hishihara, K. Furukawa, M. Kabasawa, K. Maeda, K. Miura, and H. Ohnuma, Phys. Rev. Lett. **51**, 1328 (1983).

[15] A. J. Baltz, J. Weneser, B. A. Brown, and J. Rapaport, Phys. Rev. Lett. **53**, 2078 (1984).

[16] J. D. Anderson, R. W. Bauer, V. R. Brown, S. M. Grimes, V. A. Madsen, B. A. Pohl, C. H. Poppe, and W. Scobel, Phys. Rev. C **38**, 1601 (1988).

[17] J. D. Anderson, V. R. Brown, R. W. Bauer, B. A. Pohl, C. H. Poppe, S. Stamer, E. Mordhorst, W. Scobel, S. M. Grimes, and V. A. Madsen, Phys. Rev. C **41**, 1993 (1990).

[18] Y. Holler, A. Kaminsky, B. Scharlemann, H. Krause, R. Langkau, W. Peters, G. Poppe, N. Schirm, W. Scobel, and R. Wien, Nucl. Instrum. Methods Phys. Res. Sect. A **235**, 123 (1985).

[19] E. Mordhorst, M. Trabandt, A. Kaminsky, H. Krause, and W. Scobel, Phys. Rev. C **34**, 103 (1986).

[20] M. A. Franey and W. G. Love, Phys. Rev. C **31**, 488 (1985).

[21] J. Jänecke, F. D. Becchetti, A. M. van den Berg, G. P. A. Berg, G. Brouwer, M. B. Greenfield, M. N. Harakeh, M. A. Hofstee, A. Nadasen, D. A. Roberts, R. Sawafta, J. M. Schippers, E. J. Stephenson, D. P. Stewart, and S. Y. van der Werf, Nucl. Phys. **A526**, 1 (1991).

[22] C. M. Baglin, Nucl. Data Sheets **66**, 347 (1992).

[23] W. Stoeffl (private communication).

[24] By comparing the 3° and 15° neutron time-of-flight spectra, we estimate that there is a concentration of Gamow-Teller transition strength at $\sim$4.75 MeV excitation which we could not resolve.

[25] F. Osterfeld, D. Cha, and J. Speth, Phys. Rev. C **31**, 372 (1985).

[26] H. Sakai, N. Matsuoka, T. Saito, A. Shimizu, M. Tosaki, M. Ieiri, K. Imai, A. Sukaguchi, and T. Motoboyashi, Phys. Rev. C **35**, 1280 (1987).

[27] G. J. Mathews, S. D. Bloom, and R. F. Hausman, Jr., Phys. Rev. C **28**, 1367 (1983).

[28] F. Petrovich, H. McManus, V. A. Madsen, and J. Atkinson, Phys. Rev. Lett. **22**, 895 (1969).

[29] S. D. Bloom, C. D. Goodman, S. M. Grimes, and R. F. Hausman, Phys. Lett. **107B**, 336 (1981).
[30] S. D. Bloom (private communication). We are indebted to Professor S. D. Bloom for extending the shell model calculations of ^{90}Zr (Ref. [27]) to ^{92}Zr.
[31] V. R. Brown and V. A. Madsen (private communication).
[32] D. J. Horen, R. L. Auble, J. Gomez del Campo, G. R. Satchler, R. L. Varner, J. R. Beene, Brian Lund, V. R. Brown, P. L. Anthony, and V. A. Madsen, Phys. Rev. C **47**, 629 (1993).
[33] T. N. Taddeucci, R. C. Byrd, T. A. Carey, D. E. Ciskowski, C. C. Foster, C. Gaarde, C. D. Goodman, E. Gülmez, W. Huang, D. J. Horen, J. Larsen, D. Marchlenski, J. B. McClelland, D. Prout, J. Rapaport, L. J. Rybarcyk, E. Sugarbaker, I. J. Van Heerden, and C. A. Whitten, Jr., Phys. Rev. C **42**, 935 (1990).
[34] S. M. Grimes, J. D. Anderson, J. C. Davis, R. H. Howell, C. Wong, A. W. Carpenter, J. A. Carr, and F. Petrovich, Phys. Rev. C **31**, 1679 (1985).
[35] C. Gaarde, J. S. Larsen, and J. Rapaport, in *Spin Excitation in Nuclei*, edited by F. Petrovich *et al.* (Plenum, New York, 1984), p. 65.